Selective Isotopic Labeling Resolves the Gel-to-Fluid Phase Transitions of the Individual Leaflets of a Planar-Supported Phospholipid Bilayer

Marie Richard-Lacroix,[*†] *Kayiganwa Natyvella Umuhire, Eugénie Lister, Christian Pellerin,*[*] *and Antonella Badia*[*]

Département de chimie, Centre québécois sur les matériaux fonctionnels, Université de Montréal, C.P. 6128, succursale Centre-ville, Montréal, QC H3C 3J7, Canada

ABSTRACT

Knowledge of the thermotropic phase behavior of solid-supported bilayer lipid assemblies is essential for mimicking the molecular organization and lateral fluidity of cell membranes. The gel-to-fluid phase transitions in a homologous series of single phospholipid bilayers supported on planar silicon substrates were investigated by temperature-controlled atomic force microscopy (AFM) and attenuated total reflection infrared (ATR-IR) spectroscopy to obtain complementary information at the mesoscopic and molecular scales. Symmetric bilayers of dipalmitoylphosphatidylcholine (DPPC) and vertically asymmetric bilayers comprised of a leaflet of DPPC and another of acyl-chain-deuterated DPPC (DPPC-d_{62}) were prepared by the Langmuir-Blodgett technique. The selective deuteration of one of the bilayer leaflets enabled the simultaneous monitoring by IR spectroscopy of the acyl chain melting in each leaflet via the spectrally isolated CH_2 and CD_2 stretching vibrations. Two gel-to-fluid transitions were discerned for both the symmetric and asymmetric bilayers in ultrapure water. The deuterium isotope effect observed in free-standing membranes was maintained for the supported bilayers. IR spectroscopy revealed that the melting of one leaflet promotes the disordering of the acyl chains in the adjacent one. The findings suggest that the two leaflet phase transitions do not evolve in isolation. This work sheds insight into the nature of leaflet–leaflet interactions and the thermodynamic properties of surface-confined phospholipid bilayers.

INTRODUCTION

Planar-supported phospholipid single bilayers are a type of artificial biomembrane of interest for biotechnological applications (e.g., electrooptical biosensors, microfluidic platforms, membrane microarrays) and widely utilized in biophysical investigations of membrane-associated biomolecules and interactions by surface-sensitive analytical techniques.[1-5] The physisorbed membrane typically consists of a 4–6 nm thick bilayer film of phospholipids separated from the solid hydrophilic surface (e.g., mica, silicon/silicon oxide, glass) by a 1 nm-thick water layer,[6] and is physically held at the surface by a combination of hydration, van der Waals, and electrostatic forces. Solid-supported lipid bilayers are prepared either by vesicle fusion[7, 8] or the transfer of pre-assembled lipid monolayers of defined molecular density from the air/water interface onto a substrate using the Langmuir-Blodgett or Langmuir-Blodgett/Langmuir-Schaefer deposition[9, 10]. The advantage of using the Langmuir-Blodgett and Langmuir-Schaefer techniques is the possibility to produce multilayer structures with varying layer compositions.

When working with supported lipid bilayers, it is imperative that their phase behavior, thermomechanical properties, and electrical characteristics mimic as closely as possible those of free-standing membranes. Numerous studies have however shown that the physicochemical properties of the ultrathin phospholipid bilayer are significantly affected by the underlying support.[11] Substrate effects are generally stronger for the proximal leaflet (bottom layer adjacent to the solid surface) than for the distal one (top layer in contact with the bulk aqueous solution), resulting in an asymmetry of the lipid diffusivity[12-14] and gel-to-fluid phase transition[15] between the two bilayer leaflets. From a biomimetic perspective, such differential leaflet behaviors must be accounted for as they can affect the phase structure and fluidity of the supported bilayer, and hence, the dynamics and function of the proteins and receptors inserted into it.

In-situ temperature-controlled atomic force microscopy (AFM)[16-21] and differential scanning calorimetry[22] investigations have revealed that mica-supported zwitterionic phospholipid bilayers undergo two independent (decoupled) gel-to-fluid phase transitions, involving melting of the acyl chains, in ultrapure water or at low (10^{-2} M) salt concentration. By contrast, the outer and inner leaflets in free-standing bilayers undergo a single melting transition and the thermally-induced domain formation is transbilayer symmetric.[23] One recurrent observation is that the thermal properties of the distal leaflet are similar to those of freely suspended small unilamellar vesicles (in terms of the transition temperature or transition temperature and enthalpy).[17-20] In contrast, the proximal leaflet often melts at higher temperature (2 to 15 ºC higher, depending on the system investigated) because it is stabilized by interactions between the charged lipid headgroups and mica (electrostatic) or between the lipids and the sandwiched water layer. On the other hand, some other studies have reported a single (coupled) transition.[24, 25] Seeger and coworkers subsequently investigated the effects of the ionic strength of the surrounding aqueous solution, the supported bilayer preparation temperature, and the surface properties (charge and roughness) of the substrate on the phase behavior of bilayers formed by vesicle fusion.[19, 26] They demonstrated that these experimental parameters modulate the relative strengths of the substrate–bilayer interaction and interleaflet coupling to produce either two separate phase transitions or a single transition with domains in register. The different experimental conditions used in the preparation of the supported lipid bilayers may therefore explain the contradictory observations.

Although thermally-induced physicochemical changes have indicated decoupled phase transitions, information on the extent of the interleaflet coupling and the influence of the melting of one leaflet on the other is lacking, due to the difficulty of chemically distinguishing the two leaflets. AFM is by far the most popular technique for studying phase transitions in supported lipid

bilayers because the trans-to-gauche conformational changes in the acyl chains associated with the melting transition induce a decrease in the membrane thickness that can be easily probed by the AFM tip with a nanometer lateral resolution.[15] Its main drawback is that it does not discriminate between the events occurring in the proximal and distal leaflets. Therefore, AFM imaging alone does not allow the unambiguous conclusion that the distal leaflet melts first because simultaneous changes in both leaflets may also lead to the observed thickness changes. Also, AFM does not provide data on the conformational order and orientation of the lipid acyl chains in each leaflet as a function of the temperature. Such information should provide a better understanding of the molecular dynamics in decoupled versus coupled leaflet transitions, as well as the effects of the experimental conditions. In-situ vibrational spectroscopies, such as Raman, infrared (IR), and sum frequency generation (SFG), provide information on the molecular organization in lipid assemblies and have been used to investigate the gel-to-fluid phase transition in supported bilayers.[27-29] However, attempts to date have failed to differentiate the contribution of each leaflet to the observed spectral changes, and no definitive conclusions could be reached about the lateral and vertical structure of the bilayer, and hence, the nature of the phase transition.

In this work, we employed attenuated total reflection infrared (ATR-IR) spectroscopy and AFM to investigate the thermotropic phase behavior of bilayers of dipalmitoylphosphatidylcholine (DPPC), a common phospholipid, and acyl-chain-deuterated DPPC (DPPC-d_{62}) (Scheme 1) deposited onto silicon (with a silicon oxide surface layer) using the Langmuir-Blodgett technique.[10] In particular, we used chemically asymmetric bilayers of hydrogenated and deuterated analogues to decouple the IR signals (methylene stretching vibrations) of the phospholipids in the two leaflets. This enabled us to follow simultaneously the temperature-induced trans–gauche conformational changes and acyl chain disordering in each leaflet. Both combinations (i.e., where

either the proximal or distal leaflet is deuterated) were investigated by AFM and IR to get a full picture of the system behavior at the mesoscopic and molecular scale, respectively. The complementary use of IR and AFM provides a more comprehensive view of the temperature-induced structural changes and the influence of the melting of one leaflet on the other.

EXPERIMENTAL SECTION

Materials. 1,2-dipalmitoyl-*sn*-glycero-3-phosphocholine (DPPC) and 1,2-dipalmitoyl-d_{62}-*sn*-glycero-3-phosphocholine (DPPC-d_{62}) were purchased as powders (purity >99%) from Avanti Polar Lipids (Alabaster, AL) and used without further purification. Reagent- and HPLC-grade chloroform were from A&C American Chemicals (Montreal, QC). Absolute ethanol was from Commercial Alcohols (Brampton, ON). Milli-Q water with a resistivity of 18.2 MΩ.cm and total organic carbon of ≤ 5 ppb was used as the subphase of the Langmuir-Blodgett trough and as the fluid medium in the AFM and ATR-IR investigations. Prime-grade polished silicon wafers (particles of <10 @ 0.3 μm, thickness of 500–550 μm) from WaferNet Inc. (San Jose, CA) were used as the bilayer support for the AFM investigations. Twenty-four-reflection silicon ATR crystals (parallelogram shaped with truncated 45º side edges, 52 mm × 20 mm × 2 mm, surface quality 40/20 scratch/dig) were supplied by Tydex (St. Petersburg, Russia).

Substrate Cleaning. The silicon wafers were first cut into ~20 mm × ~27 mm pieces with a diamond pen. Prior to the sample preparation, the pieces were degreased by immersing for a few minutes in a boiling solution of 1/3 (v/v) reagent-grade chloroform and 2/3 (v/v) ethanol, rinsing copiously with ethanol, and sonicating in ethanol for 5 min at room temperature. The silicon ATR crystals were degreased by rinsing four times with ethanol followed by chloroform. Both the wafer pieces and crystals were further exposed to oxygen plasma (Harrick Plasma Cleaner/Sterilizer PDC-32G) for 5 min (RF level medium). The silicon oxide surface layer thickness on the as-cleaned substrates was determined to be 4–5 nm by ellipsometry. The substrates were stored in ethanol (for not more than 1 h) and dried with nitrogen before use.

Surface Pressure–Area Isotherms and Langmuir-Blodgett Deposition. The phospholipids were dissolved in HPLC-grade chloroform to a concentration of 1 mM. A 100 μL volume of solution was spread on the water surface (area of 768 cm^2) of a computer-controlled KSV 3000 trough equipped with a roughened platinum plate attached to a surface pressure sensor (Biolin Scientific). The subphase temperature was regulated to 22.0 ± 0.5 °C with a circulation bath. After waiting 15 min for the chloroform to evaporate, the phospholipid monolayer was symmetrically compressed at a rate of 1 $Å^2$ $molecule^{-1}$ min^{-1} up to the film collapse to record surface pressure versus molecular area isotherms.

Two phospholipid monolayers were deposited onto the silicon substrates by Y-type vertical transfer. Substrates were withdrawn from or immersed into the aqueous subphase at a velocity of 5 mm min^{-1}. A monolayer was first compressed to the target pressure (i.e., 45 mN m^{-1} for DPPC and 50 mN m^{-1} for DPPC-d_{62}) and maintained at this pressure for 20 min. It was then transferred from the air/water interface onto the silicon by pulling the immersed substrate upward through the interface (upstroke). After waiting 20 min for the barrier movement and surface pressure to stabilize, the monolayer-covered silicon was vertically lowered (downstroke) through the air/phospholipid monolayer/water interface and into the aqueous subphase to prepare a symmetric DPPC bilayer. In the case of the vertically asymmetric DPPC/DPPC-d_{62} and DPPC-d_{62}/DPPC bilayers, a new monolayer was assembled at the air/water interface and deposited on the downstroke. The supported bilayers were transferred under trough water to the thermoregulated fluid cells used for AFM imaging and ATR-IR spectroscopy.

Temperature-Controlled Atomic Force Microscopy (AFM). Bilayers supported on the silicon wafer pieces were imaged under water in tapping mode with an extended Dimension 3100 scanning probe microscope and Nanoscope V controller (Bruker Nano, Santa Barbara, CA) using

microlever probes (model no. MSNL, Bruker AFM Probes, Camarillo, CA) of nominal spring constant of 0.1 N m^{-1}, resonance frequency of < 40 kHz in liquid, and a nominal tip radius of 2 nm. Temperature-controlled AFM imaging (20−50 °C range) was performed using a homemade stage with Peltier elements and temperature controller. The sample temperature was measured with a Fluke 179 digital thermometer and a K-type thermocouple maintained directly in contact with the bilayer-covered substrate. The temperature was increased by increments of 2–3 °C from 20 to 30 °C and by 0.5−1 °C from 37 to 50 °C and held at each temperature for 10 min for the system to reach thermal equilibrium before imaging. A full heating run typically lasted 10 to 12 h so that the fluid inside the AFM cell was periodically replenished (due to evaporation) with water heated to the same temperature as the remaining fluid inside the cell. A different region of the bilayer film was imaged at each temperature to avoid any change in molecular organization and/or melting behavior caused by repeated scanning of the same surface area.[30] Height images of 5.0 μm × 2.5 μm, unless specified otherwise, were simultaneously acquired at a scan rate of 0.896 Hz and resolution of 512 pixels × 256 pixels.

AFM Image Analysis. A quantitative analysis of the surface coverages of the fluid (melted) phase, solid (gel) phase, and hole defects was performed using ImageJ (NIH). The different features were marked manually. The gel-to-fluid transition temperature (T_m) of each leaflet was determined from empirical fits of the plots of the fraction of fluid or melted phase (f_{fluid}) versus temperature (T) to the sigmoidal function:

$$f_{fluid}(T) = f_{max} + \frac{f_0 - f_{max}}{1 + e^{(T - T_m)/\delta}} \quad (1)$$

where T_m is the gel-to-fluid transition temperature, δ is the transition width factor, $f_{max} = 1$, and f_0 is an initial offset which accounts for f_{fluid} being > 0 at the start of the heating experiment. This equation, except for the f_0 parameter, is analogous to the van't Hoff equation which has been used to extract the thermodynamic parameters of supported lipid bilayer melting from AFM images acquired at different temperatures.[18-20]

Temperature-Controlled Attenuated Total Reflection Infrared (ATR-IR) Spectroscopy. The phospholipid bilayer-coated silicon crystal was positioned in a vertical ATR accessory equipped with a homemade water-circulation jacket to control the sample temperature and a poly(tetrafluoroethylene) chamber to keep the crystal under MilliQ water throughout the experiments. A circulating thermostatic bath was used to control the temperature of the sample, which was measured using a thermocouple probe placed near the surface of the ATR crystal. Single-beam spectra were recorded with unpolarized light by averaging 1024 scans with a 4 cm^{-1} resolution using a Tensor 27 FT-IR spectrometer (Bruker Optics) equipped with a liquid-nitrogen-cooled HgCdTe detector. Four levels of zero filling were applied. Spectra were acquired in increments of ~2 ºC in the temperature range between 15 and 60 °C after a 5 min equilibration period at each set temperature. The DPPC bilayer was then removed from the crystal by wiping the surface with chloroform- and ethanol-soaked cotton swabs. The clean crystal was then used to record a series of background single-beam spectra under the same experimental conditions as the phospholipid bilayer-coated crystal and these were used to calculate sample absorbance spectra.

Silicon absorption saturates the IR signal at wavenumbers < ~1500 cm^{-1} but allows measurement of the bands due to the symmetric and anti-symmetric stretching modes of the CH_2 and CD_2 groups of the acyl chains of DPPC in the region between 2000 and 3000 cm^{-1}. The positions and full widths at half height of the CH_2 and CD_2 symmetric stretching bands were obtained by determining

the center of gravity of the bands at 20% of the maximal absorbance. The band widths were used to follow the evolution of the liquid or melted fraction as a function of the temperature. The anti-symmetric stretching mode was not used because the proximity of the very strong O-H stretching band of water makes it more sensitive to the background compensation. Two independent sets of data were averaged for each temperature investigated and a sigmoidal function of the same form as eq 1 was applied to extract the transition temperature from the band width–temperature data.

Orientation Quantification. The phospholipid orientation was quantified using the Harrick thin film approximation following a procedure described elsewhere[31, 32] and detailed in the Supporting Information. The first coefficient, $\langle P_2 \rangle$, of the orientation distribution function can be obtained by measuring two polarized ATR-IR spectra. Single-beam polarized spectra were measured by successively polarizing the IR beam parallel (p) and perpendicular (s) to the incident plane with a KRS-5 holographic polarizer (Optometrics). The values reported were averaged over two independent experiments. In the ATR geometry, the $\langle P_2 \rangle$ values are 0 for an isotropic distribution and 1 for a perfect orientation of the units along the normal to the substrate.

Results and Discussion

Effect of Acyl Chain Deuteration on the Surface Pressure–Area Isotherm. The compression isotherms of DPPC and DPPC-d_{62} recorded on ultrapure water at 22 ºC are shown in Figure 1 and the related monolayer characteristics are summarized in Table 1. The DPPC isotherm resembles isotherms reported in the literature.[33-35] The plateau between 6 and 8 mN m^{-1} is indicative of a first-order transition from a fluid-like liquid-expanded (LE) phase at higher molecular area to a solid-like condensed (C) phase at lower area. The monolayer collapses at ~72 mN m^{-1}, in line with

the pressures attained in previous Langmuir trough[33-35] and captive bubble surfactometer[36] studies. Deuteration of the two acyl chains of the DPPC has a significant impact on the compression isotherm. In agreement with previous reports,[37-39] DPPC-d_{62} exhibits a higher onset area (107 $Å^2$) than DPPC (92 $Å^2$) and must be compressed to higher surface pressure, i.e., ~14 mN m^{-1}, to initiate the LE-to-C transition. At a given surface pressure, the DPPC-d_{62} monolayer is in a more expanded state (lower packing density) than DPPC and collapses at lower pressure (~60 mN m^{-1}). This difference in monolayer behavior can be indicative of reduced cohesive van der Waals interactions between the deuterated acyl chains with respect to the hydrogenated ones and/or an increase in the local chain conformational disorder,[37] consistent with the lower main transition temperature (T_m, Table 1) and smaller transition enthalpy and entropy changes of aqueous dispersions (multilamellar vesicles) of DPPC-d_{62} compared to DPPC.[40]

The DPPC and DPPC-d_{62} monolayers were transferred from the air/water interface onto the silicon wafer or ATR crystal at 45 mN m^{-1} and 50 mN m^{-1}, respectively, well above their respective LE-to-C phase transition pressures. The monolayer films are in the condensed solid phase at these pressures. Although a monolayer surface pressure of 30–35 mN m^{-1} is generally believed to be appropriate to model lipids in bilayer membranes,[41, 42] we transferred the monolayers at higher pressures to limit the flip-flop or translocation of lipid molecules between leaflets and changes in the leaflet compositions of the asymmetric bilayers.[29, 43] Additionally, the solid-supported bilayer films transferred at 45 mN m^{-1} exhibit a lower defect density than those deposited at 35 mN m^{-1}.[20] DPPC-d_{62} was transferred at a higher surface pressure than DPPC to account for its more expanded state. Transfer of DPPC-d_{62} at pressures > 50 mN m^{-1} resulted in monolayer collapse. The molecular density of DPPC-d_{62} at 50 mN m^{-1} is 8% lower than that of DPPC at 45 mN m^{-1}. The corresponding lipid molecular area (Table 1) is either equivalent to or slightly smaller than the

lipid area in vesicles of gel phase DPPC of 48 Å^2.[44] Given the small differences in the lipid molecular areas (2–4 Å^2) at 35 mN m^{-1} and 45 or 50 mN m^{-1}, we do not expect a significant increase in the leaflet transition temperatures due to the higher lateral pressure. Transfer ratios of 1.0 ± 0.1 were recorded for the deposition of the proximal and distal leaflets of DPPC and DPPC-d_{62}, indicating that the molecular densities are maintained upon transfer onto the silicon wafer or ATR crystal.[45] These transfer ratios signify that solid-supported bilayers can be successfully prepared by high surface pressure transfer with the Langmuir-Blodgett technique, as also reported by others,[14, 29, 46, 47] without resorting to the Langmuir-Schaefer method for the deposition of the second leaflet[9].

Figure 2 shows the AFM height images of the bilayers in water at 21–22 ºC. These images reflect the most common morphologies observed before heating instead of the morphology of a specific bilayer composition. Most of the silicon surface is covered with a continuous all-solid (or gel) lipid phase. There are also linear depressions and hole defects (darker features) of depth of 0.2–0.5 nm. The depths of bilayer hole defects of 5.0–5.8 nm (not present in Figure 2) are comparable to the reported thicknesses of the gel phase of a single bilayer of DPPC (Figure S1 of Supporting Information).[21, 48, 49]

Symmetric DPPC Bilayers. Because the substrate surface and other experimental parameters influence the interleaflet coupling in the supported bilayer,[14, 19, 26] a bilayer of the fully hydrogenated DPPC was first analyzed by temperature-controlled AFM. AFM images recorded at selected temperatures while heating the symmetric bilayer from 21 to 49 ºC are presented in Figure 3a. The thermotropic transitions of the distal and proximal leaflets in the silicon-supported bilayer proceed in a manner similar to those of mica-supported bilayers (Figure S2).[16-18, 20] As the temperature is raised, branch-like depressions appear (36.6 °C), which are 0.7 ± 0.2 nm lower than

the surrounding solid phase. These lower features represent a local decrease of the bilayer film thickness that arises from the acyl chains of phospholipids in the fluid phase having gauche conformers (i.e., 5–7 gauche conformers per acyl chain for a DPPC membrane)[50, 51], and hence, a less extended chain configuration with respect to the all-trans conformation that predominates in the gel phase. The depth of the depressions is consistent with the 0.9 nm difference in bilayer thickness between the gel and fluid phases of fully-hydrated multilamellar membranes of DPPC determined by X-ray diffraction.[44, 52] The surface coverage of these depressions increases with increasing temperature. The image captured at 43.2 ºC shows some remaining solid material in the distal leaflet and a predominantly solid proximal leaflet with linear depressions. As the temperature is further increased, there is initially no significant change in the bilayer morphology (44.1 ºC) until ~45.2 °C when new irregularly-shaped depressions that are 0.4–0.5 nm lower than the surrounding solid phase are observable. There is a significant disparity in the domain sizes between the two leaflets at their respective phase transition temperatures.[28] The remaining solid domains melt as the temperature is raised (46.2 ºC), eventually leading to a featureless topography at 48.2 °C (image not shown).

These two distinct and successive stages of change in the bilayer morphology reveal the asymmetric thermodynamic behavior of the chemically symmetric bilayer. It is noteworthy that the solid domains observed during melting of the proximal leaflet on the silicon substrate are much smaller than those imaged on mica (Figure S2).[20] This may be related to differences in the surface roughness, surface energy, and/or negative charge density of the plasma-treated silicon wafer and freshly-cleaved mica (Table S1). The leaflet transitions appear to proceed via a grain boundary melting mechanism, where the fluid domains grow from domain boundaries and defect areas, where the lipids are less densely packed, eventually forming a uniform phase.[18, 53]

The fraction of fluid phase extracted from the AFM images of Figure 3a is plotted as a function of the temperature in Figure 4a. The plot clearly shows two gel-to-fluid transitions. The transition at lower temperature is associated with the distal leaflet and the one at higher temperature is attributable to the proximal leaflet. Consistent with prior reports,[16, 19-22, 54] the transition regions span a larger temperature interval (roughly 3–4 ºC) than that of free-standing multilamellar vesicles (< 1 ºC)[55]. The distal and proximal leaflet transition temperatures T_m's obtained from sigmoidal fits of the data (eq 1) are 42.6 and 45.5 °C, respectively (Table 2). An analysis of a DPPC bilayer deposited on mica under the same conditions gave similar transition temperatures: 42.8 ± 0.2 °C and 46.6 ± 0.1 ºC (Figure S3). These transition temperatures are close to those of bilayers transferred at 35 mN/m.[20] While the T_m values of both leaflets are higher than the T_m of multilamellar vesicles (41.4 °C)[56], the solid surface has a greater effect on the proximal leaflet transition temperature.

Asymmetric DPPC Bilayers. Having established by AFM that the as-deposited symmetric DPPC bilayers on silicon undergo two separate leaflet transitions, we now turn to the melting behavior of vertically asymmetric bilayers of DPPC and DPPC-d_{62}. For clarity, they are referred to as P_{HYD}/D_{DEU} and P_{DEU}/D_{HYD}, where P and D stand for the proximal and distal leaflets, respectively, and "HYD" and "DEU" refer to DPPC and DPPC-d_{62}. The T_m of multilamellar vesicles of DPPC-d_{62} is ~4–5 °C lower than that of vesicles of DPPC.[40, 57] As a first approximation, we expected a similar decrease in the transition temperatures of the deuterated leaflets of the supported bilayers, and hence, a larger difference between the leaflet T_m's of the P_{HYD}/D_{DEU} bilayer and a smaller difference in the case of P_{DEU}/D_{HYD} (compared to P_{HYD}/D_{HYD}).

Figure 3b shows selected AFM images for the P_{HYD}/D_{DEU} combination and corresponding plots of the fraction of the fluid phase as a function of the temperature are presented in Figure 4b. The

AFM images can be understood by analogy with those presented in Figure 3a, where around the first (distal) transition temperature there are large fluid domains of lower height, while much smaller domains are present near the second (proximal) transition. In fact, the main difference between the P_{HYD}/D_{DEU} and previous P_{HYD}/D_{HYD} sample is the chain-melting temperatures, which are 37.7 and 42.0 °C for the distal and proximal leaflets, respectively. The T_m value of D_{DEU} shows the decrease expected for the presence of deuterated versus hydrogenated acyl chains. On the other hand, the T_m of P_{HYD} also decreases by 3.5 °C compared to that of the P_{HYD}/D_{HYD} bilayer, instead of remaining the same, so that the difference between the leaflet transition temperatures ($\Delta T_m = T_m^P - T_m^D$) is roughly half of the anticipated value (Table 2). It is unlikely that this decrease in the T_m of the P_{HYD} leaflet is due to lipid flip-flop since the presence of DPPC in the D_{DEU} layer should cause it to melt at a temperature higher than expected from the deuterium isotope effect. This result is the first indication that the melting of one bilayer leaflet promotes the transition of the other one. Additionally, of significance is the five-fold increase in the transition width δ of the distal leaflet. This is akin to the three-fold broader main phase transition exhibited by multilamellar vesicles of DPPC-d_{62} compared to DPPC.[40] A similar broadening of the transition is observed when DPPC-d_{62} is in the proximal position (Table 2). There is no significant change in the transition widths of the hydrogenated DPPC leaflets of the asymmetric bilayers compared to the symmetric one. The presence of the substrate does not dampen the deuterium isotope effect. This finding is particularly significant because deuterated lipids are commonly employed in vibrational and NMR spectroscopy analyses of individual components in free-standing multicomponent biomolecular systems (refs 38, 58 are examples).

Figure 3c shows AFM images for the case of the P_{DEU}/D_{HYD} bilayer. Its surface topography evolves in much the same way with temperature as that of the P_{HYD}/D_{HYD} and P_{HYD}/D_{DEU} bilayers,

with the main difference being that the two transitions occur at temperatures that are very close to each other. Indeed, a careful look within the fluid domains formed during the first transition in the images captured at 40.9 and 41.4°C reveals the co-existence of gel and fluid domains in the underlying proximal leaflet. Significant melting has already occurred in the proximal leaflet at temperatures near the T_m of the distal layer, rendering the separation of the two events difficult. The fluid fraction–temperature plots in Figure 4c illustrate more clearly the closeness of the transition temperatures of the distal and proximal leaflets. The surface area fractions of the solid and fluid phases in the proximal leaflet at 40.9 ºC could not be determined due to the sub-micrometer size of the proximal leaflet domains and the presence of solid distal phase covering or obscuring the proximal layer. In the series of AFM images presented in Figure 3c, the first temperature for which the surface area coverage of the fluid phase in the proximal leaflet could be quantified is 41.4 ºC, where the fraction of liquid phase is already 0.49 ± 0.03 (n = 3). For this reason, the fluid fraction–temperature plot of the proximal leaflet lacks data points prior to the distal T_m. Two T_m estimates are given in Table 2, one based on the fraction of fluid phase at 41.4 ºC, and another (42.0 ± 0.5 ºC) based on a fit of the data points at temperatures $\gtrsim T_m$ (solid curve, Figure 4c). The earlier melting of the proximal leaflet is expected given the deuteration of the acyl chains.[40, 57] The transition temperature of the associated hydrogenated distal leaflet (40.9 ºC) is however lower than anticipated. The extrapolation of the P_{DEU} data to temperatures < T_m (dotted curve, Figure 4c) suggests that the onset of melting occurs at lower temperature for P_{DEU} than D_{HYD} (~37 ºC versus ~40 ºC). Our hypothesis is that melting of the underlying proximal leaflet contributes to lowering the melting temperature of the overlying distal leaflet, in line with the above-mentioned observation that the melting of one bilayer leaflet promotes the transition of the other one.

The distinct leaflet transitions observed here suggest a limited flip-flop of the lipid molecules between the leaflets.[59] Conboy and coworkers used SFG vibrational spectroscopy to evaluate the kinetics of lipid flip-flop as a function of temperature and lateral surface pressure in P_{HYD}/D_{DEU} bilayers of DPPC on fused silica prisms prepared by Langmuir-Blodgett-Schaefer.[43, 60] Their conclusion was that the exchange rate is fast (on the order of minutes) near the phase transition temperature and decreases with the lateral surface pressure/molecular density at which the lipid monolayers are transferred. At a transfer pressure of 42 mN m^{-1} (i.e., comparable to the surface pressures at which the monolayers were transferred in this work) and T_m – 4 ºC, they estimated a flip-flop half-life of 56 min (the flip-flop rate in the fluid bilayer was too fast to be measurable by SFG).[43] By contrast, a several orders of magnitude slower interleaflet exchange was found in the case of large unilamellar vesicles of DPPC, with flip-flop half-times of > 4500 h at 20 ºC (gel phase) and 105 h at 55 ºC (fluid phase).[61] The difference in the flip-flop rates of the solid-supported and free-standing phospholipid bilayers arises from a defect-mediated acceleration of lipid translocation in the supported membrane, where long-lived, submicron-sized hole defects (i.e., areas of incomplete surface coverage) are the sites of rapid interleaflet transfer,[61] consistent with the observed dependence of the flip-flop half-time on the lateral surface pressure[43]. As shown in Figure 2, the as-prepared DPPC bilayers present a low area coverage of defects ($\lesssim$ 0.5%). If the rate of lipid flip-flop was of the order of minutes near the phase transition, the equilibration of the bilayers for 10 min at each temperature before recording the AFM images (and 5 min for the upcoming IR spectra) would have homogenized the leaflet compositions and yielded the same T_m regardless of whether DPPC-d_{62} was in the proximal or distal leaflet. Our T_m results are consistent with minimal lipid exchange within the timeframe of the AFM and IR experiments.

ATR-IR spectroscopy was used to follow the thermally-induced conformational changes of the acyl chains to disentangle the phenomena occurring in the individual leaflets. The AFM height changes indicate that the melting transitions in the D_{HYD}/P_{HYD} and D_{DEU}/P_{HYD} proceed in a decoupled layer-by-layer process. We questioned whether this description was accurate by probing the molecular conformational changes occurring in the proximal leaflet during melting of the distal leaflet. Figure 5 shows IR spectra recorded at different temperatures for the P_{HYD}/D_{DEU} bilayer in ultrapure water (Figure S4 shows results for the symmetric P_{HYD}/D_{HYD} bilayer, where the overlap of the contributions from each leaflet prevent the identification of discrete phase transitions). At 20 °C, the positions of the symmetric and anti-symmetric C-H stretching bands of the CH_2 groups, centered at ~2849 and ~2918 cm^{-1}, respectively, are indicative of a predominantly trans conformation of the lipid acyl chains in the proximal leaflet.[62, 63] The symmetric and anti-symmetric C-D stretching bands of the CD_2 groups are isotopically shifted to 2090 and 2192 cm^{-1}, respectively, enabling their independent detection. Their positions at 20 °C are also consistent with a gel phase for the lipids in the deuterated distal leaflet after transfer onto the silicon ATR crystal.[64] This initially high degree of order is also confirmed by the high $\langle P_2 \rangle$ values of 0.89 and 0.80 ± 0.04 measured from polarized spectra for the distal and proximal leaflets, respectively. The acyl chain orientations in the D_{DEU} and P_{HYD} leaflets are therefore similar. Assuming a narrow unimodal orientation distribution function,[65, 66] the corresponding average tilt angles of the acyl chains with respect to the surface normal are 16 and $22 \pm 3°$ for the distal and proximal leaflets, respectively. These values concord with the tilt angles of 12–30° reported for Langmuir monolayers and solid-supported bilayers of dialkylphosphatidylcholines in the condensed or gel phase.[67-71] Overall, the $\langle P_2 \rangle$ values and tilt angles mean that the difference in the transition

temperatures of the two leaflets observed by AFM is not due to an initial difference in the conformational order or orientation of the acyl chains.

Upon increasing the temperature, the C-H and C-D stretching bands gradually shift to higher wavenumber, indicating the loss of order through a gradual conversion from trans to gauche conformation. Figure 5 also shows that both sets of bands broaden with increasing temperature. The positions and widths of the symmetric and anti-symmetric stretching bands reach a plateau at 55 °C, indicating that the transitions are complete, as expected based on the AFM measurements. While the band positions are typically used to probe order–disorder transitions spectroscopically, Dluhy and coworkers have shown that the widths of the bands are more representative of the acyl chain conformational (dis-)order in lipid bilayers.[62] Indeed, they found that changes in the peak frequency remain small until 70–80% of the lipids have melted. By contrast, the width of the bands changes more significantly in the range of 0-75% melted lipid. The two spectroscopic characteristics yielded different transition temperatures (lower temperature from band widths than from band positions) that may be associated with the different responses of these parameters to lipid melting.[62] The band widths were considered a better choice for evaluating the transition temperature of DPPC so this approach was employed here.

Figure 6 presents the evolution of the full widths at half height of the symmetric C-H and C-D stretching bands with temperature for the two types of asymmetric bilayers. As for the AFM data (Figure 4), the band width–temperature data could be fit using a sigmoidal function. The fits for the distal and proximal leaflets of the P_{HYD}/D_{DEU} bilayer give transition temperatures of 34 and 42 °C, respectively (Table 2). The melting temperature of the D_{DEU} leaflet is substantially lower than the value obtained by AFM (37.7 °C). This is not necessarily surprising considering that AFM and IR probe different aspects of the phase transition at completely different scales. More importantly,

the leaflet transitions occur over a much larger temperature span (δ ~ 4–5 ºC) compared to AFM (δ ~ 0.5–1 °C). The onset of the acyl chain disordering in the proximal leaflet coincides with the phase transition temperature of the distal leaflet (Figure 6a) and there is much greater overlap of the leaflet transitions than suggested by AFM. For instance, when the C-D band width of the distal leaflet reaches 75% of its maximum change, the C-H band width of the proximal leaflet is already at 40%. The fundamentally different structural features probed by IR and AFM can explain these important differences. Several segments in a given DPPC chain must adopt a gauche conformation to cause a decrease in thickness that is large enough to be detected by AFM. Furthermore, the lateral resolution in AFM depends on the tip radius of curvature. For the combination of tip radius (nominal 2 nm) and height difference (0.5–1 nm) that apply to this work, the width of the fluid depression must be > 2 nm.[72] This means that the acyl chains of more than 7 neighboring phospholipid molecules must melt for a thickness change to be detected by the probe tip (i.e., π(10 Å)^2/48 Å^2 molecule^{-1}). By contrast, IR spectroscopy probes the chemical environment and conformation at the molecular level, regardless of the number of trans and gauche segments in a given chain or the number of neighboring chains simultaneously experiencing the transition. The onset of molecular disorder is therefore detected at lower temperature by IR in comparison to the thickness change observed by AFM. This reasoning is also applicable at temperatures above the phase transition temperature, where the trans/gauche fraction continues to evolve, although to a lesser extent than near the transition temperature. The most direct consequence is the broadening of the melting transition observed by IR spectroscopy compared to AFM, but this can also explain the lower IR transition temperatures. Analogous differences between the molecular changes probed by IR spectroscopy and changes of the macroscopic physical state have been reported in studies of the thermally-induced phase transitions of amphiphilic polymers in aqueous solution.[73,

[74] The heating-induced spectral variations indicate that the molecular changes begin at temperatures well below the temperature of macroscopic phase separation and evolve over a wider temperature range than the macroscopic phenomena.

Figure 6b shows the progression of the C-H and C-D band widths of the P_{DEU}/D_{HYD} bilayer with temperature. The data reveal a significant coincidence of the leaflet transitions, with the deuterated proximal leaflet melting first at 33 °C and the hydrogenated distal layer later at 37 °C. The chemical selectivity of IR allows observing the transition of the proximal leaflet from its onset. The acyl chain disordering and melting of P_{DEU} at lower temperature than D_{HYD} is explicit in the IR data and substantiates the earlier transition onset suggested by the extrapolation of the AFM data in Figure 4c. Even though the AFM results indicate that the midpoint of the macroscopic phase transition occurs at higher temperature for the proximal deuterated leaflet, the IR data clearly indicate that it starts to disorganize locally at a lower temperature than the distal leaflet.

The results of AFM and IR spectroscopy (Table 2) establish that there are always two distinct transitions and thus, an asymmetric thermal behavior, regardless of the presence of deuterated lipids. The deuterated leaflet begins to melt at a lower temperature than the hydrogenated leaflet even when it is present in the proximal leaflet, in contrast with initial expectations. Notably, the conformational disordering of the deuterated leaflet lowers the transition temperature of the hydrogenated leaflet, regardless of its location. This observation implies that the leaflets do not evolve independently, and thus, that the phase transition temperature of each leaflet is sensitive to the state of (dis-)order of the adjacent layer, even when two distinct phase transitions are clearly observed.

CONCLUSIONS

Temperature-controlled AFM and IR spectroscopy reveal that silicon-supported DPPC single bilayers prepared by the Langmuir-Blodgett technique exhibit an asymmetric thermotropic phase behavior; these undergo two distinct gel-to-fluid transitions in ultrapure water. Heating-induced changes in the bilayer topography reveal that the distal leaflet melts at lower temperature and that the second transition at higher temperature is associated with the proximal leaflet. However, a comparison of the T_m's of the symmetric hydrogenated bilayer with those of the vertically asymmetric hydrogenated/deuterated systems suggests that the transition temperature of the hydrogenated leaflet is also lowered by the presence of the deuterated leaflet.

Unlike AFM, IR can simultaneously probe the molecular-scale acyl chain conformational changes due to the chemical isolation of one of the bilayer leaflets by its selective deuteration. The transition temperatures determined by IR are lower for the deuterated leaflet than for the hydrogenated leaflet, irrespective of their location, and the transitions span a much larger temperature range than observed at the mesoscopic scale by AFM. IR further reveals a greater overlap of the individual leaflet transitions than suggested by AFM. The IR and AFM results thus provide complementary information on the events leading to the gel-to-fluid transition.

Taken together, our results indicate that although two gel-to-fluid transitions are observed, this does not mean that the proximal and distal leaflets behave independently or the absence of any interleaflet coupling. On the contrary, we find that the thermotropic behavior of one leaflet affects the other, a phenomenon that becomes especially apparent when the proximal leaflet disorders first. These findings shed new light about the nature of interleaflet interactions on the thermotropic behavior of planar-supported single phospholipid bilayers. The approach used here should be useful for investigations of the phase properties and molecular dynamics of bilayers that mimic

the vertical asymmetry of lipids and proteins in the two leaflets of plasma membranes, including the impact of specific lipid and protein clustering in one leaflet on the properties of the adjacent layer.

ASSOCIATED CONTENT

Supporting Information. Surface properties of the silicon and mica substrates, depths of the bilayer deep hole defects, controlled-temperature AFM images of a mica-supported DPPC bilayer, fraction of fluid phase–temperature plots for the mica-supported DPPC bilayer, and controlled-temperature IR spectra of a silicon-supported symmetric DPPC bilayer, determination of the orientation parameter. (PDF)

AUTHOR INFORMATION

Corresponding Author

*Email: marie.richard-lacroix@uni-jena.de (M.R.-L.)

*Email: c.pellerin@umontreal.ca (C.P.)

*Email: antonella.badia@umontreal.ca (A.B.)

Present Address

†M.R.-L.: Institute of Physical Chemistry and Abbe Center of Photonics, University of Jena, Helmholtzweg 4, D-07743 Jena, Germany and Leibniz Institute of Photonic Technology (IPHT), Albert-Einstein-Straße 9, D-07745 Jena, Germany

Author Contributions

A.B., M.R.-L., and C.P. designed the experiments. K.N.U. and E.L. ran the surface pressure-area isotherms and carried out the film transfers. K.N.U. performed the temperature-controlled AFM imaging. K.N.U. and A.B. analyzed the AFM data. M.R.-L. carried out all the temperature-controlled ATR-IR measurements and IR data analysis. M.R.-L., A.B., and C.P. interpreted the data and cowrote the manuscript. All authors have given approval to the final version of the manuscript.

Notes

The authors declare no competing financial interest.

ACKNOWLEDGMENT

This research was supported by the Natural Sciences and Engineering Research Council of Canada through grant numbers RGPIN-03588-2014 (A.B.) and RGPIN-04014-2015 (C.P.) and the Alexander Graham Bell Canada Graduate Scholarships-Doctoral and Postdoctoral Fellowships programs (M.R.-L.). The authors thank the Machine and Electronics shops of the Département de chimie of the Université de Montréal for the production of the jacketed IR fluid cell and AFM heating sample stage.

REFERENCES

1. Andersson, J.; Köper, I., Tethered and Polymer Supported Bilayer Lipid Membranes: Structure and Function. *Membranes* **2016,** *6*, 30.

2. Castellana, E. T.; Cremer, P. S., Solid Supported Lipid Bilayers: From Biophysical Studies to Sensor Design. *Surf. Sci. Rep.* **2006,** *61*, 429-444.

3. Jackman, J. A.; Knoll, W.; Cho, N.-J., Biotechnology Applications of Tethered Lipid Bilayer Membranes. *Materials* **2012,** *5*, 2637-2657.

4. Kiessling, V.; Domanska, M. K.; Murray, D.; Wan, C.; Tamm, L. K., Supported Lipid Bilayers. In *Wiley Encyclopedia of Chemical Biology*, John Wiley & Sons, Inc.: Hoboken, NJ, 2008; Vol. 4, pp 411-422.

5. Parkkila, P.; Elderdfi, M.; Bunker, A.; Viitala, T., Biophysical Characterization of Supported Lipid Bilayers Using Parallel Dual-Wavelength Surface Plasmon Resonance and Quartz Crystal Microbalance Measurements. *Langmuir* **2018,** *34*, 8081-8091.

6. Zwang, T. J.; Fletcher, W. R.; Lane, T. J.; Johal, M. S., Quantification of the Layer of Hydration of a Supported Lipid Bilayer. *Langmuir* **2010,** *26*, 4598-4601.

7. Attwood, S.; Choi, Y.; Leonenko, Z., Preparation of DOPC and DPPC Supported Planar Lipid Bilayers for Atomic Force Microscopy and Atomic Force Spectroscopy. *Int. J. Mol. Sci.* **2013,** *14*, 3514-3539.

8. Lv, Z.; Banerjee, S.; Zagorski, K.; Lyubchenko, Y. L., Supported Lipid Bilayers for Atomic Force Microscopy Studies. *Methods in Molecular Biology (Clifton, N.J.)* **2018,** *1814*, 129-143.

9. Tamm, L. K.; McConnell, H. M., Supported Phospholipid Bilayers. *Biophys. J.* **1985,** *47*, 105-113.

10. Kurniawan, J.; Ventrici de Souza, J. F.; Dang, A. T.; Liu, G.-y.; Kuhl, T. L., Preparation and Characterization of Solid-Supported Lipid Bilayers Formed by Langmuir–Blodgett Deposition: A Tutorial. *Langmuir* **2018,** *34*, 15622-15639.

11. Tero, R., Substrate Effects on the Formation Process, Structure and Physicochemical Properties of Supported Lipid Bilayers. *Materials* **2012,** *5*, 2658-2680.

12. Hetzer, M.; Heinz, S.; Grage, S.; Bayerl, T. M., Asymmetric Molecular Friction in Supported Phospholipid Bilayers Revealed by NMR Measurements of Lipid Diffusion. *Langmuir* **1998,** *14*, 982-984.

13. Motegi, T.; Yamazaki, K.; Ogino, T.; Tero, R., Substrate-Induced Structure and Molecular Dynamics in a Lipid Bilayer Membrane. *Langmuir* **2017,** *33*, 14748-14755.

14. Scomparin, C.; Lecuyer, S.; Ferreira, M.; Charitat, T.; Tinland, B., Diffusion in Supported Lipid Bilayers: Influence of Substrate and Preparation Technique on the Internal Dynamics. *Eur. Phys. J. E* **2009,** *28*, 211-220.

15. Alessandrini, A.; Facci, P., Phase Transitions in Supported Lipid Bilayers Studied by AFM. *Soft Matter* **2014,** *10*, 7145-7164.

16. Charrier, A.; Thibaudau, F., Main Phase Transitions in Supported Lipid Single-Bilayer. *Biophys. J.* **2005,** *89*, 1094-1101.

17. Feng, Z. V.; Spurlin, T. A.; Gewirth, A. A., Direct Visualization of Asymmetric Behavior in Supported Lipid Bilayers at the Gel-Fluid Phase Transition. *Biophys. J.* **2005,** *88*, 2154-2164.

18. Keller, D.; Larsen, N. B.; Møller, I. M.; Mouritsen, O. G., Decoupled Phase Transitions and Grain-Boundary Melting in Supported Phospholipid Bilayers. *Phys. Rev. Lett.* **2005,** *94*, 0257011.

19. Seeger, H. M.; Marino, G.; Alessandrini, A.; Facci, P., Effect of Physical Parameters on the Main Phase Transition of Supported Lipid Bilayers. *Biophys. J.* **2009,** *97*, 1067-1076.

20. Ramkaran, M.; Badia, A., Gel-to-Fluid Phase Transformations in Solid-Supported Phospholipid Bilayers Assembled by the Langmuir–Blodgett Technique: Effect of the Langmuir Monolayer Phase State and Molecular Density. *J. Phys. Chem. B* **2014,** *118*, 9708-9721.

21. Leonenko, Z. V.; Finot, E.; Ma, H.; Dahms, T. E.; Cramb, D. T., Investigation of Temperature-Induced Phase Transitions in DOPC and DPPC Phospholipid Bilayers Using Temperature-Controlled Scanning Force Microscopy. *Biophys. J.* **2004,** *86*, 3783-3793.

22. Yang, J.; Appleyard, J., The Main Phase Transition of Mica-Supported Phosphatidylcholine Membranes. *J. Phys. Chem. B* **2000,** *104*, 8097-8100.

23. Bagatolli, L. A.; Gratton, E., A Correlation between Lipid Domain Shape and Binary Phospholipid Mixture Composition in Free Standing Bilayers: A Two-Photon Fluorescence Microscopy Study. *Biophys. J.* **2000,** *79*, 434-447.

24. Schuy, S.; Janshoff, A., Thermal Expansion of Microstructured DMPC Bilayers Quantified by Temperature-Controlled Atomic Force Microscopy. *Chem. Phys. Chem.* **2006,** *7*, 1207-1210.

25. Tokumasu, F.; Jin, A. J.; Feigenson, G. W.; Dvorak, J. A., Atomic Force Microscopy of Nanometric Liposome Adsorption and Nanoscopic Membrane Domain Formation. *Ultramicroscopy* **2003,** *97*, 217-227.

26. Seeger, H. M.; Cerbo, A. D.; Alessandrini, A.; Facci, P., Supported Lipid Bilayers on Mica and Silicon Oxide: Comparison of the Main Phase Transition Behavior. *J. Phys. Chem. B* **2010,** *114*, 8926-8933.

27. Lee, C.; Bain, C. D., Raman Spectra of Planar Supported Lipid Bilayers. *Biochim. Biophys. Acta* **2005,** *1711*, 59-71.

28. Liu, J.; Conboy, J. C., Phase Transition of a Single Lipid Bilayer Measured by Sum-Frequency Vibrational Spectroscopy. *J. Am. Chem. Soc.* **2004,** *126*, 8894-8895.

29. Wu, H.-L.; Tong, Y.; Peng, Q.; Li, N.; Ye, S., Phase Transition Behaviors of the Supported DPPC Bilayer Investigated by The Sum Frequency Generation (SGF) Vibrational Spectroscopy and Atomic Force Microscopy (AFM). *Phys. Chem. Chem. Phys.* **2016,** *18*, 1411-1421.

30. Faiss, S.; Schuy, S.; Weiskopf, D.; Steinem, C.; Janshoff, A., Phase Transition of Individually Addressable Microstructured Membranes Visualized by Imaging Ellipsometry. *J. Phys. Chem. B* **2007,** *111*, 13979-13986.

31. Picard, F.; Buffeteau, T.; Desbat, B.; Auger, M.; Pézolet, M., Quantitative Orientation Measurements in Thin Lipid Films by Attenuated Total Reflection Infrared Spectroscopy. *Biophys. J.* **1999,** *76*, 539-551.

32. Richard-Lacroix, M.; Borozenko, K.; Pellerin, C.; Bazuin, C. G., Bridging the Gap between the Mesoscopic 2D Order–Order Transition and Molecular-Level Reorganization in Dot-Patterned Block Copolymer Monolayers. *Macromolecules* **2016,** *49*, 9089-9099.

33. Zhang, H.; Fan, Q.; Wang, Y. E.; Neal, C. R.; Zuo, Y. Y., Comparative Study of Clinical Pulmonary Surfactants using Atomic Force Microscopy. *Biochim. Biophys. Acta, Biomembr.* **2011,** *1808*, 1832-1842.

34. Schief, W. R.; Touryan, L.; Hall, S. B.; Vogel, V., Nanoscale Topographic Instabilities of a Phospholipid Monolayer. *J. Phys. Chem. B* **2000,** *104*, 7388-7393.

35. Hardy, N. J.; Richardson, T. H.; Grunfeld, F., Minimising Monolayer Collapse on Langmuir Troughs. *Colloids Surf. A* **2006,** *284-285*, 202-206.

36. Crane, J. M.; Putz, G.; Hall, S. B., Persistence of Phase Coexistence in Disaturated Phosphatidylcholine Monolayers at High Surface Pressures. *Biophys. J.* **1999,** *77*, 3134-3143.

37. Vaknin, D.; Kjaer, K.; Als-Nielsen, J.; Losche, M., Structural Properties of Phosphatidylcholine in a Monolayer at the Air/Water Interface. *Biophys. J.* **1991,** *59*, 1325-1332.

38. Baldyga, D. D.; Dluhy, R. A., On the Use of Deuterated Phospholipids for Infrared Spectroscopic Studies of Monomolecular Films: A Thermodynamic Analysis of Single and Bimary Component Phospholipid Monolayers. *Chem. Phys. Lipids* **1998,** *96*, 81-97.

39. Opilik, L.; Bauer, T.; Schmid, T.; Stadler, J.; Zenobi, R., Nanoscale Chemical Imaging of Segregated Lipid Domains Using Tip-enhanced Raman Spectroscopy. *Phys. Chem. Chem. Phys.* **2011,** *13*, 9978-9981.

40. Guard-Friar, D.; Chen, C. H.; Engle, A. S., Deuterium Isotope Effect on the Stability of Molecules: Phospholipids. *J. Phys. Chem.* **1985,** *89*, 1810-1813.

41. Blume, A., A Comparative Study of the Phase Transitions of Phospholipid Bilayers and Monolayers. *Biochim. Biophys. Acta* **1979,** *557*, 32-44.

42. Marsh, D., Lateral Pressure in Membranes. *Biochim. Biophys. Acta* **1996,** *1286*, 183-223.

43. Anglin, T. C.; Conboy, J. C., Lateral Pressure Dependence of the Phospholipid Transmembrane Diffusion Rate in Planar-Supported Lipid Bilayers. *Biophys. J.* **2008,** *95*, 186-193.

44. Sun, W.-J.; Suter, R. M.; Knewtson, M. A.; Worthington, C. R.; Tristram-Nagle, S.; Zhang, R.; Nagle, J. F., Order and Disorder in Fully Hydrated Unoriented Bilayers of Gel Phase Dipalmitoylphosphatidylcholine. *Phys. Rev. E* **1994,** *49*, 4665-4676.

45. Petty, M. C., *Langmuir-Blodgett Films: An Introduction*. Cambridge University Press: New York, 1996.

46. Bassereau, P.; Pincet, F., Quantitative Analysis of Holes in Supported Bilayers Providing the Adsorption Energy of Surfactants on Solid Substrate. *Langmuir* **1997,** *13*, 7003-7007.

47. Harb, F. F.; Tinland, B., Effect of Ionic Strength on Dynamics of Supported Phosphatidylcholine Lipid Bilayer Revealed by FRAPP and Langmuir–Blodgett Transfer Ratios. *Langmuir* **2013,** *29*, 5540-5546.

48. Schuy, S.; Faiss, S.; Yoder, N. C.; Kalsani, V.; Kumar, K.; Janshoff, A.; Vogel, R., Structure and Thermotropic Phase Behavior of Fluorinated Phospholipid Bilayers: A Combined Attenuated Total Reflection FTIR Spectroscopy and Imaging Ellipsometry Study. *J. Phys. Chem. B* **2008,** *112*, 8250-8256.

49. Grandbois, M.; Clausen-Schaumann, H.; Gaub, H., Atomic Force Microscope Imaging of Phospholipid Bilayer Degradation by Phospholipase A_2. *Biophys. J.* **1998,** *74*, 2398-2404.

50. Smondyrev, A. M.; Berkowitz, M. L., Structure of Dipalmitoylphosphatidylcholine/Cholesterol Bilayer at Low and High Cholesterol Concentrations: Molecular Dynamics Simulation. *Biophys. J.* **1999,** *77*, 2075-2089.

51. Mendelsohn, R.; Davies, M. A.; Schuster, H. F.; Xu, Z.; Bittman, R., CD2 Rocking Modes as Quantitative Infrared Probes of One-, Two-, and Three-bond Conformational Disorder in Dipalmitoylphosphatidylcholine and Dipalmitoylphosphatidylcholine/Cholesterol Mixtures. *Biochemistry* **1991,** *30*, 8558-8563.

52. Nagle, J. F.; Tristram-Nagle, S., Structure of Lipid Bilayers. *Biochim. Biophys. Acta* **2000,** *1469*, 159-195.

53. Xie, A. F.; Yamada, R.; Gewirth, A. A.; Granick, S., Materials Science of the Gel to Fluid Phase Transition in a Supported Phospholipid Bilayer. *Phys. Rev. Lett.* **2002,** *89*, 2461031-2461034.

54. Garcia-Manyes, S.; Oncins, G.; Sanz, F., Effect of Temperature on the Nanomechanics of Lipid Bilayers Studied by Force Spectroscopy. *Biophys. J.* **2005,** *89*, 4261-4274.

55. Knoll, W., Calorimetric Investigations of Lipid Phase Transitions, I. The Width of Transition. *Thermochim. Acta* **1984,** *77*, 35-47.

56. Marsh, D., *CRC Handbook of Lipid Bilayers*. CRC Press: Boca Raton, FL, 1990.

57. Dorset, D. L.; Strauss, H. L.; Snyder, R. G., Chain-length Dependence of the Melting Point Difference between Hydrogenated and Deuterated Crystalline n-Alkanes. *J. Phys. Chem.* **1991,** *95*, 938-940.

58. Ramos, A. P.; Lagüe, P.; Lamoureux, G.; Lafleur, M., Effect of Saturated Very Long-Chain Fatty Acids on the Organization of Lipid Membranes: A Study Combining 2H NMR Spectroscopy and Molecular Dynamics Simulations. *J. Phys. Chem. B* **2016,** *120*, 6951-6960.

59. Allhusen, J. S.; Conboy, J. C., The Ins and Outs of Lipid Flip-Flop. *Acc. Chem. Res.* **2017,** *50*, 58-65.

60. Anglin, T. C.; Cooper, M. P.; Li, H.; Chandler, K.; Conboy, J. C., Free Energy and Entropy of Activation for Phospholipid Flip-Flop in Planar Supported Lipid Bilayers. *J. Phys. Chem. B* **2010,** *114*, 1903-1914.

61. Marquardt, D.; Heberle, F. A.; Miti, T.; Eicher, B.; London, E.; Katsaras, J.; Pabst, G., 1H NMR Shows Slow Phospholipid Flip-Flop in Gel and Fluid Bilayers. *Langmuir* **2017,** *33*, 3731-3741.

62. Dluhy, R. A.; Mendelsohn, R.; Casal, H. L.; Mantsch, H. H., Interaction of Dipalmitoylphosphatidylcholine and Dimyristoylphosphatidylcholine-d54 Mixtures with Glycophorin. A Fourier Transform Infrared Investigation. *Biochemistry* **1983,** *22*, 1170-1177.

63. Cameron, D. G.; Casal, H. L.; Mantsch, H. H., Characterization of the Pretransition in 1,2-Dipalmitoyl-sn-glycero-3-phosphocholine by Fourier Transform Infrared Spectroscopy. *Biochemistry* **1980,** *19*, 3665-3672.

64. MacPhail, R. A.; Strauss, H. L.; Snyder, R. G.; Elliger, C. A., Carbon-Hydrogen Stretching Modes and the Structure of n-Alkyl Chains. 2. Long, All-trans Chains. *J. Phys. Chem.* **1984,** *88*, 334-341.

65. Richard-Lacroix, M.; Pellerin, C., Novel Method for Quantifying Molecular Orientation by Polarized Raman Spectroscopy: A Comparative Simulations Study. *Appl. Spectrosc.* **2013,** *67*, 409-419.

66. Richard-Lacroix, M.; Pellerin, C., Accurate New Method for Molecular Orientation Quantification Using Polarized Raman Spectroscopy. *Macromolecules* **2013,** *46*, 5561-5569.

67. Garcia-Araez, N.; Brosseau, C. L.; Rodriguez, P.; Lipkowski, J., Layer-by-Layer PMIRRAS Characterization of DMPC Bilayers Deposited on a Au(111) Electrode Surface. *Langmuir* **2006,** *22*, 10365-10371.

68. Liu, J.; Conboy, J. C., Structure of a Gel Phase Lipid Bilayer Prepared by the Langmuir-Blodgett/Langmuir-Schaefer Method Characterized by Sum-Frequency Vibrational Spectroscopy. *Langmuir* **2005,** *21*, 9091-9097.

69. Behyan, S.; Borozenko, O.; Khan, A.; Faral, M.; Badia, A.; DeWolf, C., Nanoparticle-Induced Structural Changes in Lung Surfactant Membranes: An X-ray Scattering Study. *Environ. Sci.: Nano* **2018,** *5*, 1218-1230.

70. Watkins, E. B.; Miller, C. E.; Liao, W.-P.; Kuhl, T. L., Equilibrium or Quenched: Fundamental Differences between Lipid Monolayers, Supported Bilayers, and Membranes. *ACS Nano* **2014,** *8*, 3181-3191.

71. Smith, G. S.; Majewski, J., X-ray and Neutron Scattering Studies of Lipid Monolayers and Single Bilayers. In *Lipid Bilayers: Structure and Interactions*, Katsaras, J.; Gutberlet, T., Eds. Springer-Verlag: Heidelberg, 2001; pp 127–147.

72. Gan, Y., Atomic and Subnanometer Resolution in Ambient Conditions by Atomic Force Microscopy. *Surf. Sci. Rep.* **2009,** *64*, 99-121.

73. Katsumoto, Y.; Tsuchiizu, A.; Qiu, X.; Winnik, F. M., Dissecting the Mechanism of the Heat-Induced Phase Separation and Crystallization of Poly(2-isopropyl-2-oxazoline) in Water through Vibrational Spectroscopy and Molecular Orbital Calculations. *Macromolecules* **2012,** *45*, 3531-3541.

74. Percot, A.; Zhu, X.; Lafleur, M., A Simple FTIR Spectroscopic Method for the Determination of the Lower Critical Solution Temperature of N-Isopropylacrylamide Copolymers and Related Hydrogels. *J. Polym. Sci. B-Polym. Phys.* **2000,** *38*, 907-915.

Table 1. Characteristics of the Langmuir Monolayer Precursors and Layer Transfer Ratios

Lipid	T_m[vesicles40, 56] (°C)	LE-C transition pressure[a] (mN m^{-1})	Molecular area at the monolayer transfer pressure[a] (Å^2)	Transfer ratio[d]
DPPC (HYD)	41.4	6.3 ± 0.1	44 ± 1[b]	P_{HYD} = 1.1 D_{HYD} = 0.9
DPPC-d_{62} (DEU)	37.1	13.8 ± 0.2	48 ± 1[c]	P_{HYD} = 1.1 D_{DEU} = 1.0 P_{DEU} = 1.1 D_{HYD} = 1.0

[a]Values are the mean and standard deviation of 3 independent experiments. [b]Surface pressure of 45 mN m^{-1}. [c]Surface pressure of 50 mN m^{-1}. [d]Transfer ratios for bilayers whose AFM images are presented in Figure 3.

Table 2. Summary of the Gel-to-Fluid Transition Temperatures Determined by AFM and IR[a,b]

Bilayer	T_m^{AFM}	ΔT_m^{AFM}	δ^{AFM}	T_m^{IR}	ΔT_m^{IR}	δ^{IR}
			(°C)			
D_{HYD}	42.6 ± 0.03	2.9	0.2	_[c]	_	_
P_{HYD}	45.5 ± 0.1		0.4	_	_	_
D_{DEU}	37.7 ± 0.2	4.3	1	34 ± 1	8	5
P_{HYD}	42.0 ± 0.2		0.5	42 ± 1		4
D_{HYD}	40.9 ± 0.04	0.5–1.1	0.3	37 ± 1	-4	5
P_{DEU}	41.4; 42.0 ± 0.5		0.9	33 ± 1		5

[a]Errors in T_m^{AFM} are the uncertainties associated with the sigmoidal fits of the data presented in Figure 4. [b]Error in T_m^{IR} is the estimated overall uncertainty based on the analyses of the spectra. [c]Transition is not discernable.

Scheme 1. Chemical Structures of the Phospholipids Used in This Work

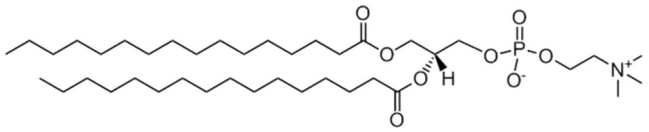

DPPC

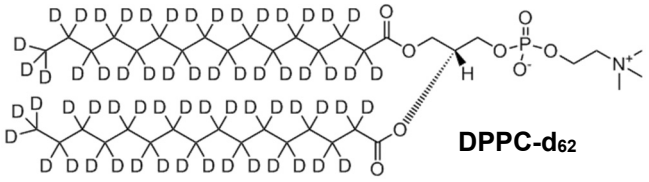

DPPC-d_{62}

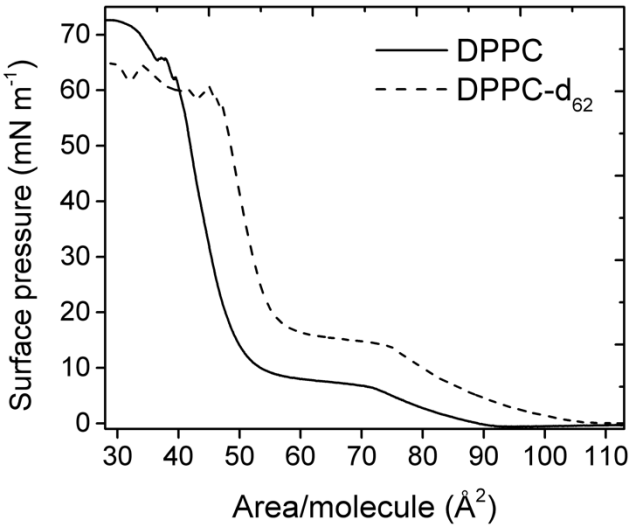

Figure 1. Surface pressure–area isotherms for DPPC and DPPC-d_{62} at 22 ºC on an ultrapure water subphase.

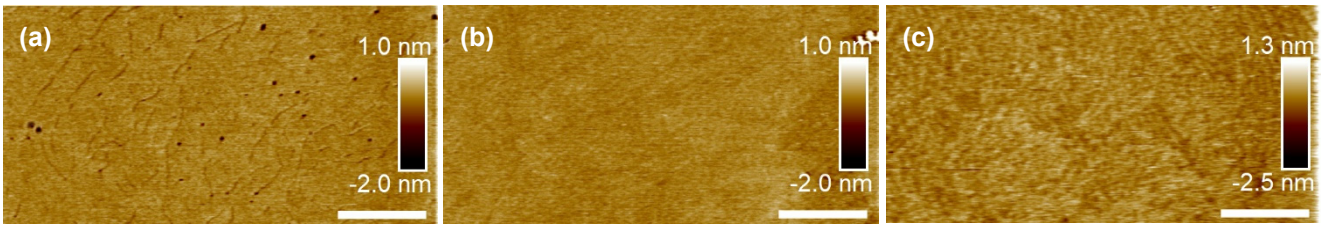

Figure 2. Representative AFM height images of silicon-supported single bilayers of DPPC at 21–22 ºC. Lipid combination (proximal layer/distal layer): (a) DPPC/DPPC, (b) DPPC/DPPC-d_{62}, and (c) DPPC-d_{62}/DPPC. Scale bar = 1 μm.

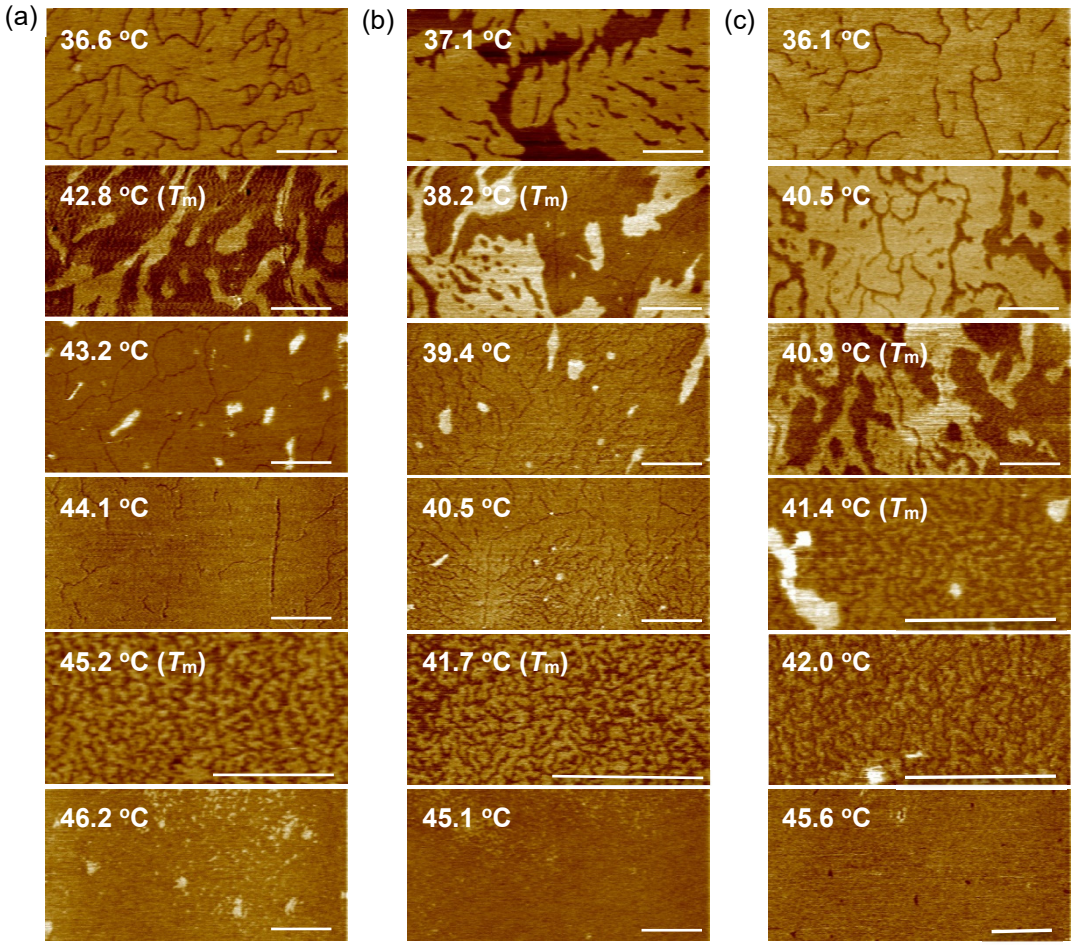

Figure 3. AFM height images captured at various temperatures while heating silicon-supported single bilayers of DPPC. Lipid combination (proximal leaflet/distal leaflet): (a) DPPC/DPPC, (b) DPPC/DPPC-d_{62}, and (c) DPPC-d_{62}/DPPC. Scale bar = 1 μm.

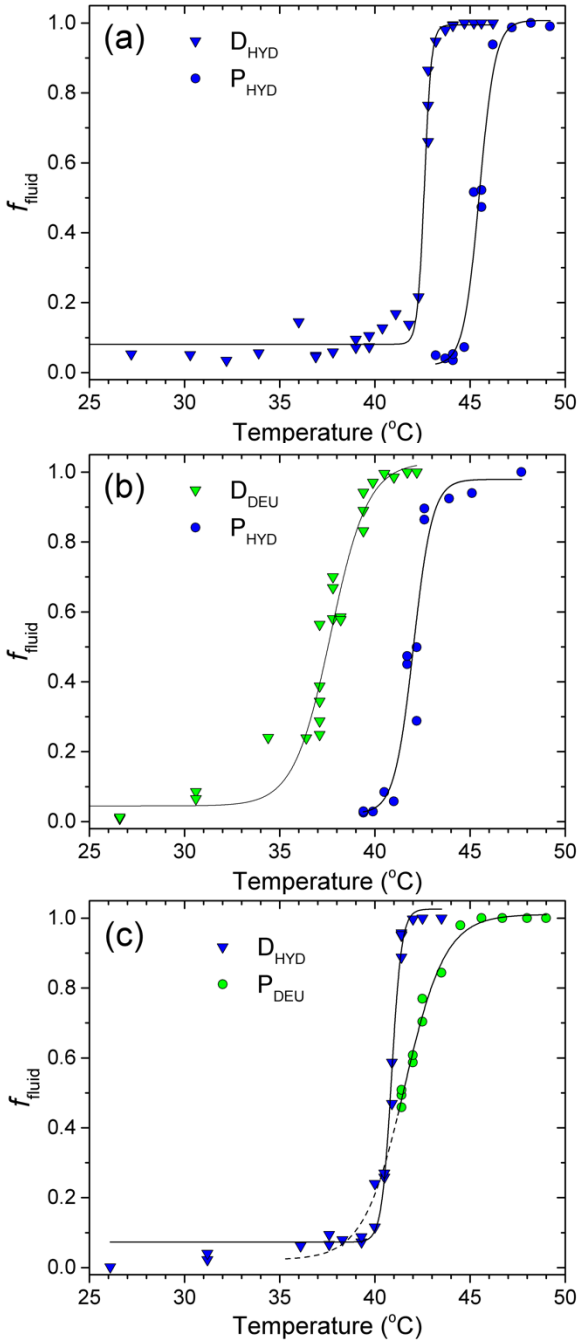

Figure 4. Area fraction of the fluid or melted phase (f_{fluid}) as a function of temperature for silicon-supported single bilayers (proximal/distal) of (a) DPPC/DPPC, (b) DPPC/DPPC-d_{62}, and (c) DPPC-d_{62}/DPPC. The f_{fluid} data is from the bilayers whose AFM images are presented in Figure 3. Triangles (▽) and circles (○) are used to designate the data of the distal and proximal leaflets,

respectively. Blue represents DPPC and green is used for DPPC-d_{62}. The black curves are fits of the data to the sigmoidal function given in eq 1. The dashed curve in (c) is an extrapolation of the f_{fluid} data of the proximal leaflet from 41 to 35 ºC.

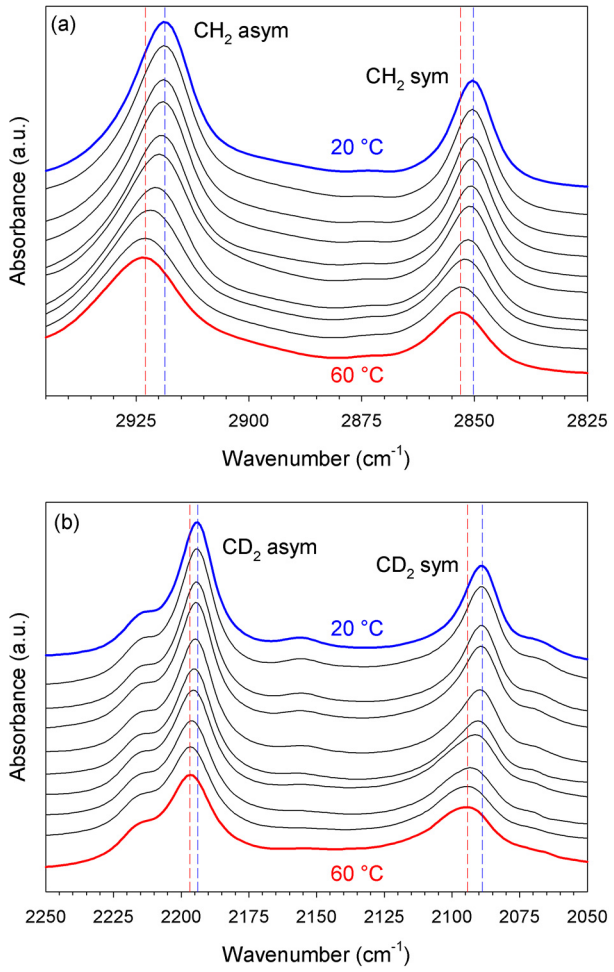

Figure 5. ATR-IR spectra in the (a) C-H and (b) C-D stretching range of the silicon-supported DPPC bilayer whose distal leaflet is comprised of deuterated DPPC (D_{DEU}) and proximal leaflet of hydrogenated DPPC (P_{HYD}). Spectra are shown from 20 to 60 °C (top to bottom). Dashed lines are visual aids.

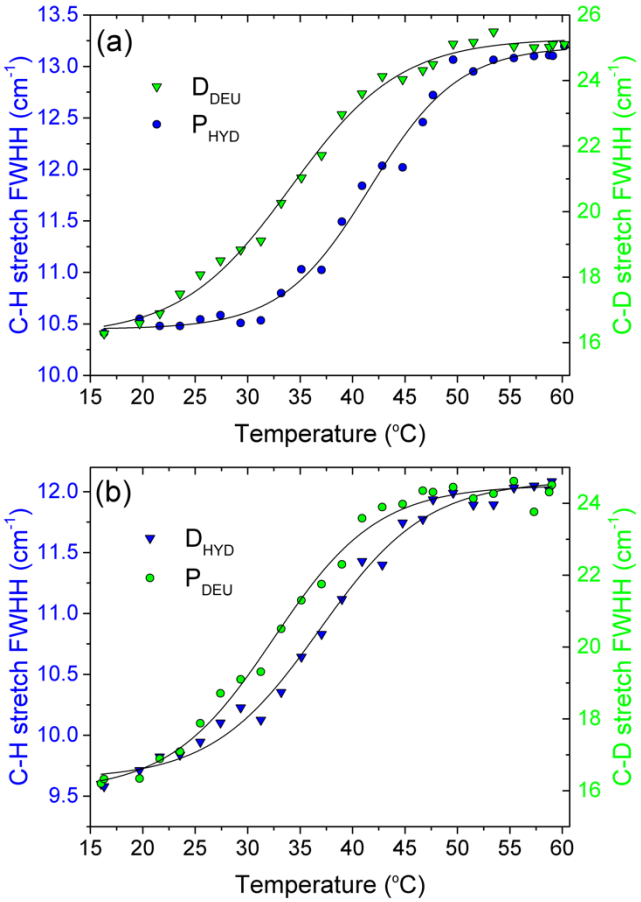

Figure 6. Full width at half height (FWHH) of the symmetric stretching band at 2850 cm^{-1} for CH_2 or 2090 cm^{-1} for CD_2 as a function of the temperature. Bilayer leaflet composition (proximal/distal): (a) DPPC/DPPC-d_{62} and (b) DPPC-d_{62}/DPPC. The black curves are sigmoidal fits of the data.

TOC Graphic